An efficient scheme on wet/dry transitions for Shallow Water Equations with friction

Christophe Berthon[a], Fabien Marche[b], Rodolphe Turpault[a]

[a]*Université de Nantes, Laboratoire de Mathmatiques Jean Leray, 2 rue de la Houssinire 44322 Nantes, France.*
[b]*Université Montpellier 2, I3M, CC051, Montpellier, France.*

Abstract

The present work concerns the derivation of a suitable discretization to approximate the friction source terms in the shallow-water model. Such additional source terms are known to be very stiff as soon as the water height is vanishing. The proposed numerical procedure comes from a relevant correction of a Godunov-type scheme that approximates the solutions of hyperbolic systems of conservation laws. The adopted correction gives a discretization of the source term which preserves the robustness and does not change the CFL condition. The scheme is shown to be particularly efficient for wet/dry transition simulations. In addition, this numerical procedure can be used together with any robust and well-balanced discretization of the topography source term. Second order extension is also investigated. Extensive numerical validations illustrate the interest of this new approach.

Keywords: Shallow-water equations, friction source term, Godunov-type schemes, hydrostatic reconstruction.

1. Introduction

The present study is devoted to the derivation of a numerical method in order to approximate the solutions of the shallow-water equations supplemented by a friction source term. The adopted model is governed by the following system:

$$\begin{aligned} &\partial_t h + \partial_x hu = 0, \\ &\partial_t hu + \partial_x (hu^2 + \frac{gh^2}{2}) = -ghb'(x) - \frac{\kappa |hu|}{h^\eta} hu, \end{aligned} \tag{1}$$

where h is the local water depth and u is the depth-averaged velocity. Here, we have set $g > 0$ the gravity constant. Concerning the source terms, $b : \mathbf{R} \to \mathbf{R}^+$ is a given smooth function which describes the topography, while κ and η are two given positive friction parameters.

For the sake of clarity in the notations, it turns out to be useful to rewrite (1) in the following condensed-form:

$$\partial_t U + \partial_x G(U) = -\mathcal{B}(U) - \mathcal{F}(U),$$

where we have set:

$$U = \begin{pmatrix} h \\ hu \end{pmatrix}, \; G(U) = \begin{pmatrix} hu \\ hu^2 + \dfrac{gh^2}{2} \end{pmatrix}, \tag{2}$$

$$\mathcal{B}(U) = \begin{pmatrix} 0 \\ ghb'(x) \end{pmatrix} \text{ and } \mathcal{F}(U) = \begin{pmatrix} 0 \\ \dfrac{\kappa |hu|}{h^\eta} hu \end{pmatrix}. \tag{3}$$

As usual, the state vector is assumed to belong to the convex set of admissible states Ω defined as follows:

$$\Omega = \{U \in \mathbf{R}^2 / h \geq 0, \; u \in \mathbf{R}\}. \tag{4}$$

During the last decade, the numerical approximation of the solutions of the shallow-water model was widely studied and several numerical procedures have been developed. Most of them derive from the well-balanced strategy introduced by Greenberg and LeRoux [16]. Their main idea concerns the relevance of the source term discretization versus the approximation of the first order operator. The main objective is there to preserve the steady-state solution given by:

$$\begin{aligned} &hu = cte, \\ &\frac{h^2}{2} + gh + gb = cte, \end{aligned}$$

and the most famous of them is nothing but the lake at rest:

$$u = 0 \text{ and } h + b = cte. \tag{5}$$

Several schemes are thus developed in this spirit (for instance, see [6, 14, 18, 25, 9, 7] and references therein). In [1], the authors propose a suitable well-balanced interpretation: the so-called hydrostatic reconstruction. This approach allows an easy implementation of source terms (such as topography) which also ensures required robustness properties. In addition, such a technique allows an efficient treatment of the dry areas ($h = 0$).

To improve the numerical simulation of shallow-water experiments, the topography source term $\mathcal{B}$ must be supplemented by the friction source-term $\mathcal{F}$ given by (3). For instance, a real-life model can be found in [19]. The main discrepancy between both source terms comes from their relevance in dry regions. Indeed, the friction term is not a priori bounded for small water heights. Since a numerical control of the friction term is not reachable, wet/dry transitions are very difficult to simulate.

Such a remark eliminates most of source term splitting strategies and more sophisticate approaches must be investigated to approximate $\mathcal{F}$. For instance, in [11] an extension of the hydrostatic reconstruction is derived for the friction term. Such a technique is very efficient but a particular attention must be paid to wet/dry transitions.

Here, we propose a derivation of a new source term discretization based on an appropriate correction. More precisely, we will adopt the well-known approximate Riemann solver of Harten, Lax and Van Leer [17] on the following hyperbolic system of conservation laws:

$$\partial_t U + \partial_x G(U) = 0, \tag{6}$$

where the state vector $U \in \Omega$ and the flux function $G(U) : \Omega \to \mathbf{R}^2$ are given by (2).

Next, we will introduce a correction directly into the Riemann solver to make the discretization consistent with the following hyperbolic system with source term:

$$\partial_t U + \partial_x G(U) = -\mathcal{F}(U),$$

where $\mathcal{F}$ is the required friction term. One of the main edges of the derived numerical scheme concerns the robustness since it preserves the nonnegativity of h without involving any additional restriction.

The paper is organized as follows: in the next section, the proposed source term correction and the resulting scheme are exposed. The main properties of the resulting method are given. Next, in section 3, we consider a second-order MUSCL extension to increase the order of accuracy in space. This extension is proved to be robust and to preserve the non-negativity of the water height. Section 4 concerns the introduction of the topography source term. As explained above, we adopt the hydrostatic reconstruction to deal with $\mathcal{B}(U)$. Once again, the robustness of the scheme is established. In addition, the whole scheme is shown to be well-balanced since it preserves the lake at rest. Finally, section 5 is devoted to numerous simulations that illustrate the interest of the scheme.

2. Friction discretization

The goal of this section is to design a numerical scheme to approximate the solutions of the shallow-water equations with friction. Let us recall that these equations are given by the following system:

$$\partial_t h + \partial_x hu = 0, \tag{7}$$

$$\partial_t hu + \partial_x (hu^2 + \frac{gh^2}{2}) = -\frac{\kappa |hu|}{h^\eta} hu. \tag{8}$$

Involving (2) and (3), this system rewrites:

$$\partial_t U + \partial_x G(U) = -\mathcal{F}(U). \tag{9}$$

To approximate the system (7)-(8), we propose to modify any suitable Godunov-type scheme associated to the shallow-water equations (6). To do so, we first introduce a finite volume scheme in the formalism of Harten, Lax and Van Leer [17] to approximate the weak solutions of (6). This scheme is convenient all the more since one knows the associated approximate Riemann solver. Then we propose a relevant modification of this approximate Riemann solver to build a scheme which takes into account the friction term. The resulting scheme will be shown to preserve the positivity of h under the CFL condition imposed by the initial chosen Godunov-type scheme.

2.1. The initial approximate Riemann solver

We consider a finite volume method approximations of the weak solutions of (6). Several strategies can be adopted and the reader is referred to Godlewski and Raviart [15] (see also [21, 29]). In the present work, we propose to consider the formalism detailed by Harten, Lax and Van Leer in [17]. For the sake of completeness, we briefly recall this approach here.

Let us consider a uniform mesh of constant size $\Delta x = x_{i+\frac{1}{2}} - x_{i-\frac{1}{2}}$, $i \in \mathbb{Z}$ and we denote Δt the time step with $t^{n+1} = t^n + \Delta t$ for all $n \in \mathbb{N}$.

Let us assume that a piecewise constant approximation $U^{\Delta x}(x, t^n) \in \Omega$ of the solution at time t^n is known:

$$U^{\Delta x}(x, t^n) = U_i^n \text{ if } x \in (x_{i-\frac{1}{2}}, x_{i+\frac{1}{2}}).$$

To evolve this approximation in time, we consider an approximate Riemann solver stated at each interface $x_{i+\frac{1}{2}}$. This approximate Riemann solver, denoted by $U_{\mathcal{R}}(\frac{x}{t}; U_L, U_R)$ is built as follows:

$$U_{\mathcal{R}}\Big(\frac{x}{t}; U_L, U_R\Big) = \begin{cases} U_L, \text{ if } \frac{x}{t} < a^-, \\ U^\star(\frac{x}{t}; U_L, U_R), \text{ if } a^- < \frac{x}{t} < a^+, \\ U_R, \text{ if } \frac{x}{t} > a^+, \end{cases} \tag{10}$$

where a^- and a^+ are respectively the minimum and maximum velocity waves involved by the approximate Riemann solver. Furthermore, the intermediate state $U^\star$, describes the approximate solution inside the dependence cone characterized by $x = a^- t$ and $x = a^+ t$. Following [17], we recall that the approximate Riemann solver (10) must satisfy a consistency condition given by:

$$\frac{1}{\Delta x} \int_{-\frac{\Delta x}{2}}^{\frac{\Delta x}{2}} U_{\mathcal{R}}\Big(\frac{x}{\Delta t}; U_L, U_R\Big) dx = \frac{1}{2}(U_L + U_R) - \frac{\Delta t}{\Delta x}\Big(G(U_R) - G(U_L)\Big), \tag{11}$$

where Δt is restricted by the CFL-like condition:

$$\frac{\Delta t}{\Delta x} \max(|a^-|, |a^+|) \leq \frac{1}{2}.$$

There are many choices for (10) that can be found in the literature (see for instance [6, 17, 28, 4]). Let us note that the exact Godunov scheme enters the proposed definition with a^- and a^+ the exact minimum and maximum characteristic speeds and $U^\star(x/t)$ is the exact Riemann solution into the dependence cone. Another example involves the famous one-intermediate state HLL scheme [17] where $U^\star(x/t)$ is given by the following constant:

$$U^\star\Big(\frac{x}{t}; U_L, U_R\Big) = \frac{a^+ U_R - a^- U_L}{a^+ - a^-} - \frac{1}{a^+ - a^-}\Big(G(U_R) - G(U_L)\Big).$$

The HLLC proposed by [28] (see [29, 2] for several examples and extensions) and the relaxation schemes [4, 6, 22] also enter such a framework.

Now an approximate Riemann solver $U_{\mathcal{R}}(\frac{x - x_{i+\frac{1}{2}}}{t}; U_L, U_R)$

is stated at each cell interface $x_{i+\frac{1}{2}}$. We thus obtain a non-interacting juxtaposition of Riemann solvers as soon as the following CFL-like condition is assumed:

$$\frac{\Delta t}{\Delta x}\max_{i\in\mathbb{Z}}(|a^-_{i+\frac{1}{2}}|, |a^+_{i+\frac{1}{2}}|) \leq \frac{1}{2}. \tag{12}$$

Then we define an approximate solution at time $t^n + t$ for all $t \in (0, \Delta t)$ as follows:

$$U^{\Delta x}(x, t^n + t) = U_{\mathcal{R}}\Big(\frac{x - x_{i+\frac{1}{2}}}{t}; U_i^n, U_{i+1}^n\Big) \text{ if } x \in (x_i, x_{i+1}). \tag{13}$$

The projection of this solution on the piecewise constant functions gives the expected updated approximation:

$$U_i^{n+1} = \frac{1}{\Delta x}\int_{x_{i-\frac{1}{2}}}^{x_{i+\frac{1}{2}}} U^{\Delta x}(x, t^n + \Delta t)dx. \tag{14}$$

Introducing the condition (11), the scheme can be rewritten into a standard conservation form:

$$U_i^{n+1} = U_i^n - \frac{\Delta t}{\Delta x}\Big(G_{i+\frac{1}{2}} - G_{i-\frac{1}{2}}\Big), \tag{15}$$

where we have:

$$G_{i+\frac{1}{2}} = G(U_i^n) + \frac{\Delta x}{2\Delta t}U_i^n - \frac{1}{\Delta t}\int_{x_i}^{x_{i+\frac{1}{2}}} U_{\mathcal{R}}\Big(\frac{x - x_{i+\frac{1}{2}}}{\Delta t}; U_i^n, U_{i+1}^n\Big)dx. \tag{16}$$

Finally, the resulting scheme perserves the positivity of h. This property is stated in the following result:

Lemma 1. *Let U_L and U_R be two constant states such that h_L, $h_R \geq 0$. Assume that for all $a^- < \frac{x}{t} < a^+$, $U^\star(\frac{x}{t}; U_L, U_R) \in \Omega$. Then, under the CFL restriction (12), as soon as $h_i^n \geq 0$ for all $i \in \mathbb{Z}$, we have $h_i^{n+1} \geq 0$ for all $i \in \mathbb{Z}$.*

We skip the proof of this classical result (see for instance [2, 6] for further details).

2.2. Extension to include the friction term

We now correct the above approximate Riemann solver to take into account the friction terms involved in (8). To do so, we adapt a recent asymptotic preserving numerical procedure [5, 3] to our problem (see also [10] for another approach). We modify the intermediate state $U^\star = (h^\star, (hu)^\star)^T$ by introducing a new intermediate state vector $\tilde{U}^\star$ defined as follows:

$$\tilde{U}^\star(x/t; U_L, U_R) = \begin{cases} U^\star(x/t; U_L, U_R) + (1-\alpha)\Big(U_L^\star(\frac{x}{t}; U_L, U_R) \\ \quad - U^\star(\frac{x}{t}; U_L, U_R) - \dfrac{h_L^\eta}{\kappa (hu)_{ref}}\mathcal{F}(U_L)\Big), \\ \hfill \text{if } x/t < 0, \\ U^\star(x/t; U_L, U_R) + (1-\alpha)\Big(U_R^\star(\frac{x}{t}; U_L, U_R) \\ \quad - U^\star(\frac{x}{t}; U_L, U_R) - \dfrac{h_R^\eta}{\kappa (hu)_{ref}}\mathcal{F}(U_R)\Big), \\ \hfill \text{if } x/t > 0, \end{cases}$$

where we have set:

$$U_L^\star(\frac{x}{t}; U_L, U_R) = \begin{pmatrix} h^\star(\frac{x}{t}; U_L, U_R) \\ h_L u_L \end{pmatrix} \text{ and}$$
$$U_R^\star(\frac{x}{t}; U_L, U_R) = \begin{pmatrix} h^\star(\frac{x}{t}; U_L, U_R) \\ h_R u_R \end{pmatrix}.$$

Here $\alpha \in [0, 1]$ is a parameter that will be defined later through consistency conditions. Furthermore, $(hu)_{ref}$ is a dimensioning constant which will be set to 1 in the following.

Let us emphasize that the first component of $\tilde{U}^\star$ stays unchanged since $\tilde{h}^\star(\frac{x}{t}; U_L, U_R) = h^\star(\frac{x}{t}; U_L, U_R)$. On the other hand, the second component of $\tilde{U}^\star$ reads:

$$(\tilde{hu})^\star(x/t; U_L, U_R) = \begin{cases} \alpha(hu)^\star(x/t; U_L, U_R) \\ \quad + (1-\alpha)(h_L u_L - |h_L u_L| h_L u_L), \\ \hfill \text{if } x/t < 0, \\ \alpha(hu)^\star(x/t; U_L, U_R) \\ \quad + (1-\alpha)(h_R u_R - |h_R u_R| h_R u_R), \\ \hfill \text{if } x/t > 0. \end{cases}$$

With this correction of the intermediate state, the modified approximate Riemann solver is now given by:

$$\tilde{U}_{\mathcal{R}}(x/t; U_L, U_R) = \begin{cases} U_L \text{ if } x/t < a^-, \\ U^\star + (1-\alpha)(U_L^\star - U^\star - \frac{h^\eta}{\kappa}\mathcal{F}(U_L)) \\ \hfill \text{if } a^- < x/t < 0, \\ U^\star + (1-\alpha)(U_R^\star - U^\star - \frac{h^\eta}{\kappa}\mathcal{F}(U_R)) \\ \hfill \text{if } 0 < x/t < a^+, \\ U_R \text{ if } x/t > a^+. \end{cases} \tag{17}$$

where a^- and a^+ were introduced in (10). While we have assumed in the above equation that $a^- < 0 < a^+$ for the sake of clarity, the reader is referred to [5] for the extension to any pair (a^-, a^+).

Once again, we then consider the juxtaposition of the Riemann solvers stated at each interface. Such a juxtaposition is non-interacting as long as Δt satisfies the CFL-like condition (12). Then, at time $t^n + t$ for all $t \in (0, \Delta t)$, the juxtaposition of non-interacting approximate Riemann solutions reads as follows:

$$\tilde{U}^{\Delta x}(x, t^n + t) = \tilde{U}_{\mathcal{R}}\Big(\frac{x - x_{i+\frac{1}{2}}}{t}; U_i^n, U_{i+1}^n\Big), \text{ if } x \in (x_i, x_{i+1}).$$

As usual, the updated states are mean values of the solution at time $t + \Delta t$ inside each cell:

$$U_i^{n+1} = \frac{1}{\Delta x}\int_{x_{i-\frac{1}{2}}}^{x_{i+\frac{1}{2}}} \tilde{U}^{\Delta x}(x, t^n + \Delta t)dx. \tag{18}$$

This integral formulation can be developed to write the scheme under a conservation form supplemented by a relevant discretization of the source term. Indeed, plugging (17) into (18) we have:

$$
\begin{aligned}
U_i^{n+1} &= \frac{1}{\Delta x}\int_{x_{i-\frac12}}^{x_{i+\frac12}} U^{\Delta x}(x,t^n+\Delta t)dx \\
&+ \frac{1-\alpha_{i-\frac12}}{\Delta x}\int_{x_{i-\frac12}}^{x_{i-\frac12}+a^+_{i-\frac12}\Delta t}\Big(U^\star_{R,i-\frac12} - U^\star_{i-\frac12} - \frac{(h_i^n)^\eta}{\kappa}\mathcal{F}(U_i^n)\Big)dx \\
&+ \frac{1-\alpha_{i+\frac12}}{\Delta x}\int_{x_{i+\frac12}-a^-_{i+\frac12}\Delta t}^{x_{i+\frac12}}\Big(U^\star_{L,i+\frac12} - U^\star_{i+\frac12} - \frac{(h_i^n)^\eta}{\kappa}\mathcal{F}(U_i^n)\Big)dx,
\end{aligned}
$$

where we have set:

$$
\begin{aligned}
U^\star_{L,i+\frac12} &= \begin{pmatrix} h^\star\big(\frac{x-x_{i+\frac12}}{\Delta t}; U_i^n, U_{i+1}^n\big) \\ h_i^n u_i^n \end{pmatrix}, \\
U^\star_{R,i-\frac12} &= \begin{pmatrix} h^\star\big(\frac{x-x_{i-\frac12}}{\Delta t}; U_{i-1}^n, U_i^n\big) \\ h_i^n u_i^n \end{pmatrix}, \\
U^\star_{i+\frac12} &= \begin{pmatrix} h^\star\big(\frac{x-x_{i+\frac12}}{\Delta t}; U_i^n, U_{i+1}^n\big) \\ (hu)^\star\big(\frac{x-x_{i+\frac12}}{\Delta t}; U_i^n, U_{i+1}^n\big) \end{pmatrix}.
\end{aligned}
$$

Using the definition of $U^{\Delta x}$ given by (13) and the consistency condition (11), a straightforward computation leads to:

$$
h_i^{n+1} = h_i^n - \frac{\Delta t}{\Delta x}\Big(G^h_{i+\frac12} - G^h_{i-\frac12}\Big), \tag{19}
$$

$$
\begin{aligned}
(hu)_i^{n+1} &= (hu)_i^n - \frac{\Delta t}{\Delta x}\Big(\alpha_{i+\frac12}G^{hu}_{i+\frac12} - \alpha_{i-\frac12}G^{hu}_{i-\frac12}\Big) \\
&\quad - \Delta t\Big(\frac{1-\alpha_{i-\frac12}}{\Delta x}a^+_{i-\frac12} + \frac{1-\alpha_{i+\frac12}}{\Delta x}a^-_{i+\frac12}\Big)|h_i^n u_i^n| h_i^n u_i^n \\
&\quad + \frac{\Delta t}{\Delta x}(\alpha_{i-\frac12} - \alpha_{i+\frac12})\Big(h_i^n(u_i^n)^2 + \frac{g(h_i^n)^2}{2}\Big),
\end{aligned} \tag{20}
$$

where $G_{i+\frac12} = (G^h_{i+\frac12}, G^{hu}_{i+\frac12})^T$ is defined by (16).

To conclude the definition of this numerical scheme, we need to define the parameter $\alpha_{i+\frac12}$. As previously stated, we consider consistency conditions in order to do so. In particular, $\alpha_{i+\frac12}$ shall fulfill the following requirements:

- No friction limit: $\alpha_{i+\frac12} = 1$ whenever $\kappa = 0$,
- High friction limit: $\alpha_{i+\frac12} \to 0$ in the limit of $\kappa \to \infty$,
- Source term consistency: $\frac{1-\alpha_{i+\frac12}}{\Delta x} = \frac{\kappa}{h^\eta} + o(1)$,
- Dry conditions: $\alpha_{i+\frac12}$ must be defined even if $h = 0$,
- $\alpha_{i+\frac12} \in [0;1]$.

Additional constraints on α may be considered in order to build high-order schemes or other specific properties.

Among the admissible choices of $\alpha_{i+\frac12}$, we choose to consider the following one:

$$
\alpha_{i+\frac12} = \frac{(h^n_{i+\frac12})^\eta(a^+_{i+\frac12} - a^-_{i+\frac12})}{(h^n_{i+\frac12})^\eta(a^+_{i+\frac12} - a^-_{i+\frac12}) + \kappa\Delta x}, \text{ with } h^n_{i+\frac12} = \frac{h_i^n + h_{i+1}^n}{2}, \tag{21}
$$

The robustness property stated in lemma 1 is obviously preserved since the water height h_i^n is still given by the scheme (19), which is nothing but the first component of (15). Moreover, let us emphasize that the scheme is stable under the CFL condition (12) since our modification to include the source term does not change the dependency cone. This gives an important edge to this approach compared to usual source terms treatments.

To conclude the presentation of the scheme, let us note that the proposed Riemann-solver correction introduced a residual term given by:

$$
\frac{1}{\Delta x}(\alpha_{i-\frac12} - \alpha_{i+\frac12})\Big(h_i^n(u_i^n)^2 + \frac{g(h_i^n)^2}{2}\Big).
$$

In fact, it is essential to remark that, according to the consistency requirement imposed on $\alpha_{i+\frac12}$, this term is consistent with zero and never perturbes the solution or shock discontinuities (see numerical results below).

3. Second-order MUSCL extension

We now propose a second-order extension of the scheme (19)-(20) to increase the space accuracy. It is obtained by involving a MUSCL reconstruction technique as suggested by Van Leer in [20]. The purpose of this method consists in substituting a linear reconstruction for the piecewise constant approximation. At each side of the interface located at $x_{i+\frac12}$, the two reconstructed states will be denoted by $U_{i,R}$ and $U_{i+1,L}$. The accurate numerical flux function $\tilde G_{i+\frac12}$ is easily deduced from (16) by considering these two reconstructed states:

$$
\tilde G_{i+\frac12} = G(U^n_{i,R}) + \frac{\Delta x}{2\Delta t}U^n_{i,R} - \frac{1}{\Delta t}\int_{x_i}^{x_{i+\frac12}} U_{\mathcal{R}}\Big(\frac{x - x_{i+\frac12}}{\Delta t}; U^n_{i,R}, U^n_{i+1,L}\Big)dx. \tag{22}
$$

The second-order scheme is obtained by replacing $G_{i+\frac12}$ by $\tilde G_{i+\frac12} = (\tilde G^h_{i+\frac12}, \tilde G^{hu}_{i+\frac12})^T$ in (19)-(20). The MUSCL scheme thus reads:

$$
h_i^{n+1} = h_i^n - \frac{\Delta t}{\Delta x}\Big(\tilde G^h_{i+\frac12} - \tilde G^h_{i-\frac12}\Big), \tag{23}
$$

$$
\begin{aligned}
(hu)_i^{n+1} &= (hu)_i^n - \frac{\Delta t}{\Delta x}\Big(\alpha_{i+\frac12}\tilde G^{hu}_{i+\frac12} - \alpha_{i-\frac12}\tilde G^{hu}_{i-\frac12}\Big) \\
&\quad - \Delta t\Big(\frac{1-\alpha_{i-\frac12}}{\Delta x}a^+_{i-\frac12} + \frac{1-\alpha_{i+\frac12}}{\Delta x}a^-_{i+\frac12}\Big)|h_i^n u_i^n| h_i^n u_i^n \\
&\quad + \frac{\Delta t}{\Delta x}(\alpha_{i-\frac12} - \alpha_{i+\frac12})\Big(h_i^n(u_i^n)^2 + \frac{g(h_i^n)^2}{2}\Big),
\end{aligned} \tag{24}
$$

where $\alpha_{i+\frac12}$ and $a^\pm_{i+\frac12}$ are defined by using the reconstructed states. Let us recall that additional constraints on α may be considered in order to build higher-order schemes.

A large literature is devoted to reconstruction techniques. For instance, the reader is referred to LeVeque [21] where several strategies are described e.g. minmod, superbee, Van Leer limiters... Let us now focus on the robustness of the method. Indeed, we have the following statement:

Lemma 2. *Assume that* $\forall i \in \mathbb{Z}$, $h_i^n \geq 0$ *and the MUSCL reconstruction preserves the nonnegativity of the water height (i.e.* $U^n_{i,L/R} \in \Omega$*). In addition, assume that* $U_{\mathcal{R}}(\frac{x}{\Delta t}; U_L, U_R)$ *stays in* Ω *for all* $U_{L/R} \in \Omega$*. Finally, assume that the reconstructed water height satisfies:*

$$\frac{1}{2}(h^n_{i,L} + h^n_{i,R}) = h^n_i. \tag{25}$$

Then, the updated states $(U_i^{n+1})_i$ *defined by the MUSCL scheme (23)-(24) belongs to* Ω *as soon as the following half CFL condition holds:*

$$\frac{\Delta t}{\Delta x} \max_{i \in \mathbb{Z}} (|a^-_{i+\frac{1}{2}}|, |a^+_{i+\frac{1}{2}}|) \leq \frac{1}{4}.$$

Proof. Let us recall that we denote $U^h_{\mathcal{R}}$ the first component of $U_{\mathcal{R}}$. Since h_i^{n+1} is given by (23), from (22) we have:

$$\begin{aligned} h_i^{n+1} =& h_i^n + \frac{1}{2}(h^n_{i-1,R} - h^n_{i,R}) - \frac{\Delta t}{\Delta x}(G^h(U^n_{i,R}) - G^h(U^n_{i-1,R})) \\ &+ \frac{1}{\Delta x}\int_{x_i}^{x_{i+\frac{1}{2}}} U^h_{\mathcal{R}}\Big(\frac{x - x_{i+\frac{1}{2}}}{\Delta t}; U^n_{i,R}, U^n_{i+1,L}\Big)dx \\ &- \frac{1}{\Delta x}\int_{x_{i-1}}^{x_{i-\frac{1}{2}}} U^h_{\mathcal{R}}\Big(\frac{x - x_{i-\frac{1}{2}}}{\Delta t}; U^n_{i-1,R}, U^n_{i,L}\Big)dx. \end{aligned} \tag{26}$$

Involving the consistency condition (11), we can write:

$$\begin{aligned} \frac{1}{\Delta x}\int_{x_{i-1}}^{x_{i-\frac{1}{2}}} & U^h_{\mathcal{R}}\Big(\frac{x - x_{i-\frac{1}{2}}}{\Delta t}; U^n_{i-1,R}, U^n_{i,L}\Big)dx = \\ & -\frac{1}{\Delta x}\int_{x_{i-\frac{1}{2}}}^{x_i} U^h_{\mathcal{R}}\Big(\frac{x - x_{i-\frac{1}{2}}}{\Delta t}; U^n_{i-1,R}, U^n_{i,L}\Big)dx \\ & + \frac{1}{2}(h^n_{i-1,R} + h^n_{i,L}) - \frac{\Delta t}{\Delta x}(G^h(U^n_{i,L}) - G^h(U^n_{i-1,R})). \end{aligned}$$

We plug this quantity into (26) to deduce from (25) the following relation:

$$\begin{aligned} h_i^{n+1} =& \frac{1}{\Delta x}\int_{x_i}^{x_{i+\frac{1}{2}}} U^h_{\mathcal{R}}\Big(\frac{x - x_{i+\frac{1}{2}}}{\Delta t}; U^n_{i,R}, U^n_{i+1,L}\Big)dx \\ &+ \frac{1}{\Delta x}\int_{x_{i-\frac{1}{2}}}^{x_i} U^h_{\mathcal{R}}\Big(\frac{x - x_{i-\frac{1}{2}}}{\Delta t}; U^n_{i-1,R}, U^n_{i,L}\Big)dx \\ &- \frac{\Delta t}{\Delta x}(G^h(U^n_{i,R}) - G^h(U^n_{i,L})). \end{aligned} \tag{27}$$

Since we have considered an half-CFL condition, we obtain:

$$\begin{aligned} \frac{1}{\Delta x}\int_{x_i}^{x_{i+\frac{1}{2}}} & U^h_{\mathcal{R}}\Big(\frac{x - x_{i+\frac{1}{2}}}{\Delta t}; U^n_{i,R}, U^n_{i+1,L}\Big)dx \\ =& \frac{1}{\Delta x}\int_{x_i}^{x_{i+\frac{1}{4}}} U^h_{\mathcal{R}}\Big(\frac{x - x_{i+\frac{1}{2}}}{\Delta t}; U^n_{i,R}, U^n_{i+1,L}\Big)dx \\ &+ \frac{1}{\Delta x}\int_{x_{i+\frac{1}{4}}}^{x_{i+\frac{1}{2}}} U^h_{\mathcal{R}}\Big(\frac{x - x_{i+\frac{1}{2}}}{\Delta t}; U^n_{i,R}, U^n_{i+1,L}\Big)dx, \qquad (28) \\ =& \frac{1}{4}h^n_{i,R} + \frac{1}{\Delta x}\int_{x_{i+\frac{1}{4}}}^{x_{i+\frac{1}{2}}} U^h_{\mathcal{R}}\Big(\frac{x - x_{i+\frac{1}{2}}}{\Delta t}; U^n_{i,R}, U^n_{i+1,L}\Big)dx, \qquad (29) \end{aligned}$$

and similarly:

$$\begin{aligned} \frac{1}{\Delta x}\int_{x_{i-\frac{1}{2}}}^{x_i} & U^h_{\mathcal{R}}\Big(\frac{x - x_{i-\frac{1}{2}}}{\Delta t}; U^n_{i-1,R}, U^n_{i,L}\Big)dx \\ =& \frac{1}{4}h^n_{i,L} + \frac{1}{\Delta x}\int_{x_{i-\frac{1}{2}}}^{x_{i-\frac{1}{4}}} U^h_{\mathcal{R}}\Big(\frac{x - x_{i-\frac{1}{2}}}{\Delta t}; U^n_{i-1,R}, U^n_{i,L}\Big)dx. \end{aligned} \tag{30}$$

In addition, using once again the consistency condition (11) we get:

$$\begin{aligned} \frac{1}{4}(h^n_{i,L} + h^n_{i,R}) &- \frac{\Delta t}{\Delta x}(G^h(U^n_{i,R}) - G^h(U^n_{i,L})) \\ &= \frac{2}{\Delta x}\int_{x_{i-\frac{1}{4}}}^{x_{i+\frac{1}{4}}} U^h_{\mathcal{R}}\Big(\frac{x - x_i}{\Delta t}; U^n_{i,L}, U^n_{i,R}\Big)dx. \end{aligned} \tag{31}$$

By using (29), (30) and (31) into (27), we obtain:

$$\begin{aligned} h_i^{n+1} =& \frac{1}{\Delta x}\int_{x_{i+\frac{1}{4}}}^{x_{i+\frac{1}{2}}} U^h_{\mathcal{R}}\Big(\frac{x - x_{i+\frac{1}{2}}}{\Delta t}; U^n_{i,R}, U^n_{i+1,L}\Big)dx \\ &+ \frac{1}{\Delta x}\int_{x_{i-\frac{1}{2}}}^{x_{i-\frac{1}{4}}} U^h_{\mathcal{R}}\Big(\frac{x - x_{i-\frac{1}{2}}}{\Delta t}; U^n_{i-1,R}, U^n_{i,L}\Big)dx \\ &+ \frac{2}{\Delta x}\int_{x_{i-\frac{1}{4}}}^{x_{i+\frac{1}{4}}} U^h_{\mathcal{R}}\Big(\frac{x - x_i}{\Delta t}; U^n_{i,L}, U^n_{i,R}\Big)dx. \end{aligned}$$

Since each integral is nonnegative, the proof is completed.

4. Discretization of the topography

This section is devoted to the approximation of the topography source term $\mathcal{B}$ defined by (3). To obtain a high order well-balanced scheme preserving the steady-states at rest (5), we adopt the hydrostatic reconstruction proposed in [1] and extended to higher order of accuracy in [25].

Considering the cell $[x_{i-\frac12}, x_{i+\frac12}]$, we compute the MUSCL reconstruction $U^n_{i,L}$ and $U^n_{i,R}$ located at $x^+_{i-\frac12}$ and $x^-_{i+\frac12}$. Values of $H^n_{i,L}$ and $H^n_{i,R}$, where $H = h + b$, are also constructed so that we deduce reconstructions of the topography $b_{i,L} = H^n_{i,L} - h^n_{i,L}$ and $b_{i,R} = H^n_{i,R} - h^n_{i,R}$. This ensures that if, for all $i \in \mathbb{Z}$, $u^n_i = 0$ and $h^n_i + b_i = h^n_{i+1} + b_{i+1}$ then $u^n_{i,L} = u^n_{i,R} = 0$ and $H^n_{i,L} = H^n_{i,R} = h^n_i + b_i$.

Next, we perform the hydrostatic reconstruction of the values at each side of the mesh interfaces taking into account the variations of the bottom. Topography values $b_{i+\frac12}$ are defined as follows:

$$b_{i+\frac12} = \max(b_{i,R}, b_{i+1,L}).$$

The reconstruction of the water height on each side of the considered interface is defined by:

$$\begin{aligned} h^n_{i+\frac12,-} &= \max(0, h^n_{i,R} + b_{i,R} - b_{i+\frac12}),\\ h^n_{i+\frac12,+} &= \max(0, h^n_{i+1,L} + b_{i+1,L} - b_{i+\frac12}). \end{aligned}$$

We then deduce the complete reconstructed values on each side of the interface:

$$U^n_{i+\frac12,-} = \begin{pmatrix} h^n_{i+\frac12,-} \\ h^n_{i+\frac12,-} u^n_{i,R} \end{pmatrix}, \; U^n_{i+\frac12,+} = \begin{pmatrix} h^n_{i+\frac12,+} \\ h^n_{i+\frac12,+} u^n_{i+1,L} \end{pmatrix}.$$

Involving these new reconstructed values, the numerical flux is defined as follows:

$$\tilde{G}^\star_{i+\frac12} = G(U^n_{i+\frac12,-}) + \frac{\Delta x}{2\Delta t} U^n_{i+\frac12,-} \tag{32}$$

$$- \frac{1}{\Delta t} \int_{x_i}^{x_{i+\frac12}} U_{\mathcal{R}}\Big(\frac{x - x_{i+\frac12}}{\Delta t}; U^n_{i+\frac12,-}, U^n_{i+\frac12,-}\Big) dx. \tag{33}$$

Motivated by balancing requirements for static flows, the source term $\mathcal{B}(U)$ is discretized as follows:

$$\begin{aligned} \mathcal{B}^n_i = &\begin{pmatrix} 0 \\ \frac{g}{2}(h^n_{i+\frac12,-})^2 - \frac{g}{2}(h^n_{i,R})^2 \end{pmatrix} \\ &+ \begin{pmatrix} 0 \\ g\frac{h^n_{i,L}+h^n_{i,R}}{2}(b_{i,L} - b_{i,R}) \end{pmatrix} + \begin{pmatrix} 0 \\ \frac{g}{2}(h^n_{i,L})^2 - \frac{g}{2}(h^n_{i-\frac12,+})^2 \end{pmatrix}. \end{aligned}$$

We thus obtain the full scheme which approximates the solutions of the system (1):

$$h^{n+1}_i = h^n_i - \frac{\Delta t}{\Delta x}\Big(\tilde{G}^{\star,h}_{i+\frac12} - \tilde{G}^{\star,h}_{i-\frac12}\Big), \tag{34}$$

$$\begin{aligned} (hu)^{n+1}_i = (hu)^n_i &- \frac{\Delta t}{\Delta x}\Big(\alpha_{i+\frac12}\tilde{G}^{\star,hu}_{i+\frac12} - \alpha_{i-\frac12}\tilde{G}^{\star,hu}_{i-\frac12}\Big) \\ &- \Delta t\Big(\frac{1-\alpha_{i-\frac12}}{\Delta x} a^+_{i-\frac12} + \frac{1-\alpha_{i+\frac12}}{\Delta x} a^-_{i+\frac12}\Big)|h^n_i u^n_i| h^n_i u^n_i \\ &+ \frac{\Delta t}{\Delta x}(\alpha_{i-\frac12} - \alpha_{i+\frac12})\Big(h^n_i (u^n_i)^2 + \frac{g(h^n_i)^2}{2}\Big) + (\mathcal{B}^{hu})^n_i. \end{aligned} \tag{35}$$

This scheme is now established to be robust and well-balanced.

Theorem 1. *Let us consider the assumptions stated in lemma 2. Then, as soon as $(U^n_i)_i$ stay in Ω, the updated states $(U^{n+1}_i)_i$ defined by (34)-(35) belongs to Ω.*

Moreover, assume an initial data given for all $i \in \mathbb{Z}$ by $u^0_i = 0$ and $h^0_i + b_i = H$ where $H > 0$ is a given constant. Then, this steady state is preserved by the scheme: for all $i \in \mathbb{Z}$ and $n > 0$, $u^n_i = 0$ and $h^n_i + b_i = H$.

Proof. Since the scheme is nonnegative preserving as soon as for all $i \in \mathbb{Z}$ $b_i = 0$, the robustness is preserved for varying topography $b_i \geq 0$ by applying the result of Audusse et al [1].

We now prove that the scheme (34)-(35) is well-balanced. Let us assume that the approximate solution at time t^n is given by $u^n_i = 0$ and $h^n_i + b_i = H$ to write:

$$h^n_{i+\frac12,-} = \max(0, H - b_{i+\frac12}) = h^n_{i+\frac12,+},$$

and by construction:

$$U^n_{i+\frac12,-} = \begin{pmatrix} h^n_{i+\frac12,-} \\ 0 \end{pmatrix} = \begin{pmatrix} h^n_{i+\frac12,+} \\ 0 \end{pmatrix} = U^n_{i+\frac12,+}.$$

Considering (34)-(35)-(32), we immediately obtain:

$$\begin{aligned} h^{n+1}_i &= h^n_i, \\ (hu)^{n+1}_i &= 0, \end{aligned}$$

which implies the expected preservation of the steady states.

Extensive numerical investigations clearly assess these properties. All classical benchmarks for the well-balanced properties, like those found in [1] for instance, are successfully validated, but not exhibited in the following.

5. Numerical validation

This section is devoted to the numerical assessment of the new scheme introduced above. For all the following computations, we use the robust relaxation-VFRoe scheme introduced in [4], together with a second order MUSCL conservative reconstruction (34)-(35). Time discretization relies on a classical second-order Runge-Kutta scheme. Time step are evaluated at each iteration in agreement with the CFL restriction (12).

We emphasize that no numerical trick is used to account for vanishing water height. We introduce a threshold value for the numerical definition of a dry cell, denoted by ε. This limiting water height is arbitrary chosen and numerical investigations have shown that when ε is small enough, the numerical results do not depend on its value. During the computations, when the water height is found to be smaller than ε in a given cell, the corresponding velocity is arbitrary set to zero. In the following computations, we set $\varepsilon = 10^{-20}$.

Also, for applications shown in the following and when nothing else is mentioned, we use the experimentally validated Manning-Chezy formulation [13] for the friction term :

$$\mathcal{F}(U) = \begin{pmatrix} 0 \\ \frac{n^2|hu|}{h^{10/3}} hu \end{pmatrix}, \tag{36}$$

corresponding to the choices $\kappa = n^2$ and $\eta = \frac{10}{3}$ in (3).
In some particular situations, it may be important to ensure that the flow may be arrested by large enough friction force but not be reversed by them. To ensure this property, a simple friction force limitation is proposed in [8]. This limitation has also been successfully applied in [23], together with a semi-implicit discretization of the friction source term. This limitation procedure can of course also be applied within our new approach, if needed.

5.1. Accuracy validation

This test is devoted to the analysis of the accuracy. We consider shallow-water equations with Manning-Chezy friction term (36). Adapting the relevant test case initially introduced by Xing and Shu [30],we use:

$$\begin{aligned} b(x) &= \sin^2(\pi x), \\ h(x,0) &= 5 + \exp(\cos(2\pi x)), \\ hu(x,0) &= \sin(\cos(2\pi x)), \end{aligned}$$

for topography, initial free surface and discharge. Periodic boundary conditions are used. Since the exact solution is not known explicitly for this case, we use the second order MUSCL scheme with $N = 25600$ points to compute a reference solution. Then, when computing the numerical errors obtained on coarser meshes, this reference solution is considered as the reference solution and sampled on the coarser meshes. We compute up to $t = 0.1\ s$ and use a Manning friction coefficient $n = 2$.
Computations are performed with the second order accurate scheme and Table 1 contains the L^2 errors and the corresponding orders of accuracy are shown on Figure 1. We clearly see that second order of accuracy is achieved, for both water height h and discharge hu, on this particular test.

Lastly, Figure 2 shows time series of the L^∞-norm for the discharge, for increasing values of $\kappa = n^2$, in order to highlight the good behavior of this new approach for large values of κ. We clearly observe that the discharge vanishes for any value of κ. In addition, higher values of κ lead to a very rapid decreasing of the velocity in the whole domain, followed by an asymptotic regime. No numerical instabilities are observed for the larger values of κ. When κ becomes very large, the system (1) degenerates into a p-Laplacian type equation. The scheme (34)-(35) was not designed to preserve this asymptotic regime. If necessary, such a property can be restored using the technique used in [5].

Number of cells	L^2-error for h	L^2-error for hu
50	$3.87\,10^{-3}$	$6.98\,10^{-2}$
100	$1.37\,10^{-3}$	$2.38\,10^{-2}$
200	$4.01\,10^{-4}$	$7.08\,10^{-3}$
400	$1.17\,10^{-4}$	$2.04\,10^{-3}$
800	$3.03\,10^{-5}$	$5.48\,10^{-4}$
Order	1.9	1.9

Table 1: Test 1 - Convergence study: relative L^2-error table for conservative variables

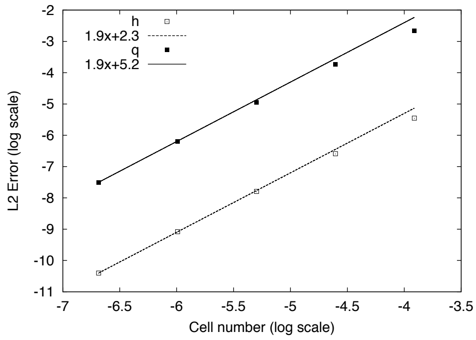

Figure 1: Test 1 - convergence analysis

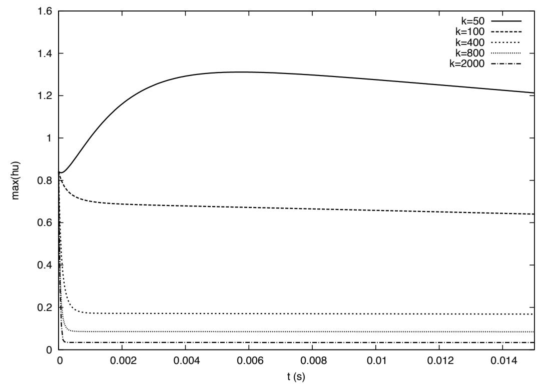

Figure 2: Test 1 - Time series of L^∞-norm for the discharge for increasing values of $\kappa = n^2$

5.2. Moving boundary over quadratic bottom

In this test, we consider moving boundary forced flow, with time oscillating shoreline, over a quadratic bottom. An analytical solution is obtained in [27] for shallow water equations with linear friction term:

$$\partial_t h + \partial_x hu = 0,$$
$$\partial_t hu + \partial_x (hu^2 + \frac{gh^2}{2}) = -\kappa hu,$$

where κ is assumed to be constant. For this particular linear friction source term, we have adapted the scheme (34)-(35) with $\eta = 0$ and $\mathcal{F}^{hu} = \kappa hu$. This test involves time oscillations of a perturbed flow in a one-dimensional quadratic basin, involving a wet/dry interface. The free surface is always planar during the oscillations. Of course the displacement of the fluid from equilibrium gradually vanishes over time, due to friction and the solution converges towards a motionless steady state.
Considering a $4320\,m$ long computational domain, the topography is defined as follows

$$b(x) = 1 - h_0 \left(\frac{x}{a}\right)^2, \quad x \geq 0,$$

and the flow is forced at the left boundary :

$$h(t,0) = \frac{a^2B^2e^{-\kappa t}}{8g^2h_0}\left(-s\kappa\sin(2st) + (\frac{\kappa^2}{4} - s^2)\cos(2st)\right) - \frac{B^2e^{-\kappa t}}{4g},$$

where h_0 and a are constants. The analytical solution for the free surface is given by:

$$h(t,x) = \frac{a^2B^2e^{-\kappa t}}{8g^2h_0}\left(-s\kappa\sin(2st) + (\frac{\kappa^2}{4} - s^2)\cos(2st)\right) - \frac{B^2e^{-\kappa t}}{4g}$$
$$-\frac{e^{-\frac{\kappa t}{2}}}{g}\left(Bs\cos(st) + \frac{\kappa B}{2}\sin(st)\right)x, \tag{37}$$

with $s = \sqrt{p^2 - \kappa^2}$ and $p = \sqrt{8gh_0/a^2}$. The velocity is obtained with

$$u(t) = Be^{-\frac{\kappa t}{2}}\sin st. \tag{38}$$

The location of the shoreline can be obtained with

$$x = \frac{a^2e^{-\frac{\kappa t}{2}}}{2gh_0}\left(-Bs\cos(st) - \frac{\kappa B}{2}\sin(st)\right) + a.$$

We compare our MUSCL scheme with this solution. The chosen values are $h_0 = 10\,m$, $a = 3000\,m$, $\kappa = 0.001\,s^{-1}$ and $B = 2\,m.s^{-1}$. Note that the period of the trigonometric terms in the motion is $1353\,s$. The initial velocity is $0\,m.s^{-1}$. The computation is performed until $t = 10000\,s$. The CFL is set to 0.8 and a regular mesh of 500 points, corresponding to $dx = 8.64\,m$, is used to obtain free surface profiles at several time during the evolution, on Figure 3. Time series of the shoreline motion can also be observed on Figure 4. Numerical results and analytical solutions are in very close agreement and the convergence towards a motionless steady state is accurately computed.

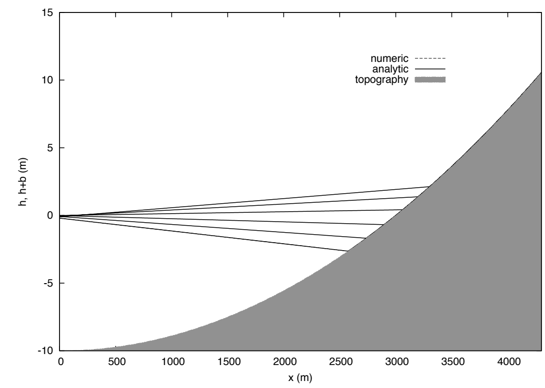

Figure 3: Test 2 - Moving boundary over quadratic bottom. Free surface profiles at several times during a half period: t=0s, t=200s, 300s, 400s, 500s and 676s.

Next, a convergence analysis is performed, as in the previous case. Table 2 contains the L^2 errors and corresponding numerical orders of accuracy for conservative variables. Convergence order of 1.3 and 1.2 are reached; respectively for h and hu, as shown on Figure 5 where the mean slopes are evaluated by a least-square method. This relative loss of accuracy, when compared to the previous case, is usual is test involving dry areas, due to the errors entailed by the very small values of h.

5.3. Moving boundary over parabolic bottom

We now consider the moving boundary fluid evolution for shallow water equations with linear friction term introduced in [26]. This solution describes time oscillations of a free boundary perturbed flow in a one-dimensional parabolic basin, involving wet/dry interfaces. Again, the free surface is always planar during the oscillations and as in the previous case, the fluid motion decays over time, due to friction damping. We again define the domain topography with

$$b(x) = 1 - h_0 \left(\frac{x}{a}\right)^2,$$

where h_0 and a are constants, but this time the computational domain is $10000\,m$ long. The analytical solutions for the

Number of cells	L^2-error for h	L^2-error for hu
50	$3.77\,10^{-3}$	$1.03\,10^{-2}$
100	$1.82\,10^{-3}$	$4.25\,10^{-3}$
200	$7.49\,10^{-4}$	$2.11\,10^{-3}$
400	$3.18\,10^{-4}$	$9.15\,10^{-4}$
800	$1.33\,10^{-4}$	$4.53\,10^{-4}$
Order	1.3	1.2

Table 2: Test 2 - Convergence study: relative L^2-error table for conservative variables

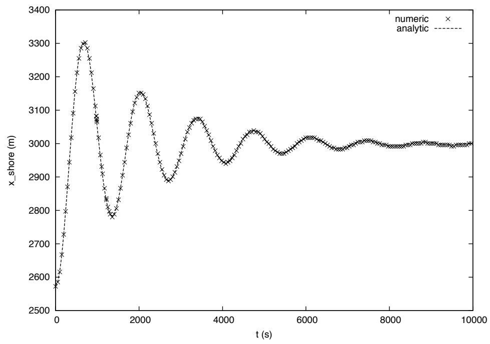

Figure 4: Test 2 - Moving boundary over quadratic bottom. Time series of the wet/dry interface location: analytic vs numeric.

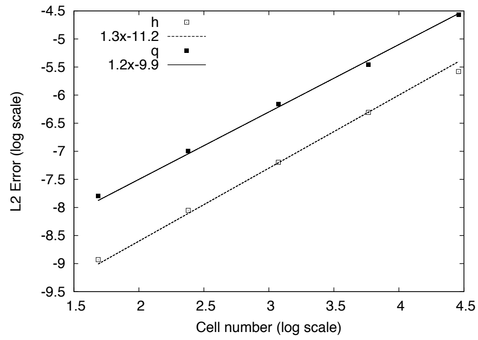

Figure 5: Test 2 - Moving boundary over quadratic bottom. Convergence curve in logarithm scale.

free surface and velocity are given by (37)-(38) and the time-evolving locations of the 2 shorelines can be obtained with

$$x = \frac{a^2 e^{-\frac{\kappa t}{2}}}{2gh_0}\left(-Bs\cos(st) - \frac{\kappa B}{2}\sin(st)\right) \pm a.$$

Again, we compare our second order accurate numerical scheme with these analytical solutions. The chosen values are $h_0 = 10\,m$, $a = 3000\,m$, $\kappa = 0.001\,s^{-1}$ and $B = 5\,m.s^{-1}$. The CFL is set to 0.8 and a regular mesh of 1000 points, corresponding to $dx = 10\,m$, is used. Free surface profiles at several times during the evolution are plotted on Figure 6. Again, we can observed that the curves corresponding respectively to numerical results and exact solutions are almost indistinguishable. To help quantifying numerical error, time series of L^2-error for the water height are shown on Figure 7, until $t = 10000\,s$. We emphasize that the L^2-error is clearly decreasing with respect to time.

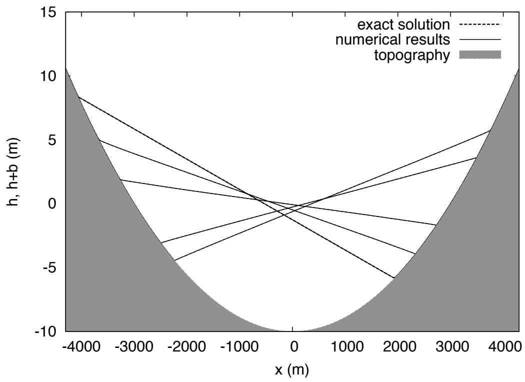

Figure 6: Test 3 - moving boundary over parabolic bottom. Free surface profiles at several times during a half period: t=0s, t=200s, t=300s, t=500s, t=676?5s

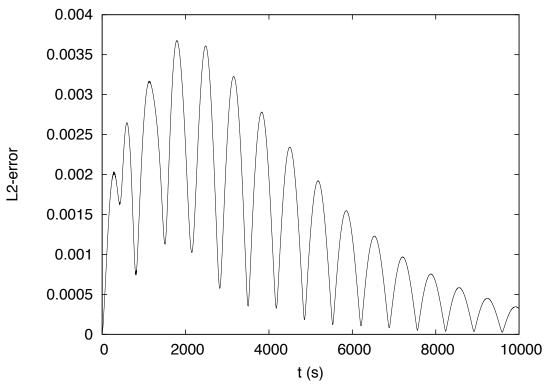

Figure 7: Test 3 - moving boundary over parabolic bottom. L^2-error time series for the water height.

Note this test case is also used in [23], with a classical semi-implicit discretization of the friction source term and a new well-balanced discretization for the topography source term, allowing some comparisons between the two approaches.

5.4. Periodic subcritical flow

In this test, we consider a subsonic solution for the shallow water equations with a Manning-Chezy friction term (36). The purposes of this test are manifold. First, we want to assess the ability of this new scheme to converge toward a steady state. In the meantime, we want to show that our approach leads to robust computations, even when considering source terms (3) that become very stiff as the water height vanishes. Considering a classical fractional step approach for the discretization of such friction terms, some numerical tricks have to be introduced to allow robust computations [23], as the source term grows very rapidly when h vanishes. Also, it is shown in [11] that more recent well-balanced approaches [6] can lead to spurious oscillations near the wet/dry interfaces.
In this test, following the lines of [24] and [12, 11], a reference solutions can be obtained for steady state flows over varying topographies. Considering a $5000\,m$ long computational domain, the steady state for the free surface considered here is given by:

$$h_{ref}(x) = \frac{9}{8} + \frac{1}{4}\sin\left(\frac{\pi x}{500}\right),$$

and we compute the corresponding topography profile with a high order iterative method [11]. The reference solutions used here are computed with 5000 cells. The steady discharge is constant on the whole domain and equal to $2\,m.s^{-1}$. Since the flow is subcritical both upstream and downstream, a discharge of $2\,m.s^{-1}$ is imposed at the left inlet boundary, while the water height is forced to $h_{ref}(5000)$ at the right outlet boundary. The initial free surface is set to zero on the whole domain. During the transient part, we observe on Figure 8 the flooding of the whole domain. We observe very robust computations of the wet/dry front motions.
We show on Figure 9 the steady state water free surface at $t = 5000\,s$. In these computations, the CFL is set to 0.8, we use 400 points and the Manning friction coefficient is $n = 0.03$. We observe very close agreement between numerical results and the reference solution.

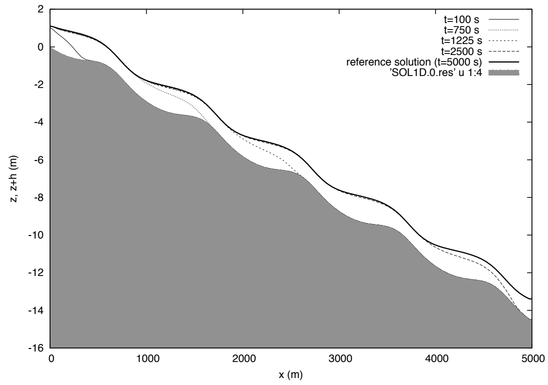

Figure 8: Test 4 - Periodic subcritical flow: transient solution. Free surface elevation at several times during the flooding.

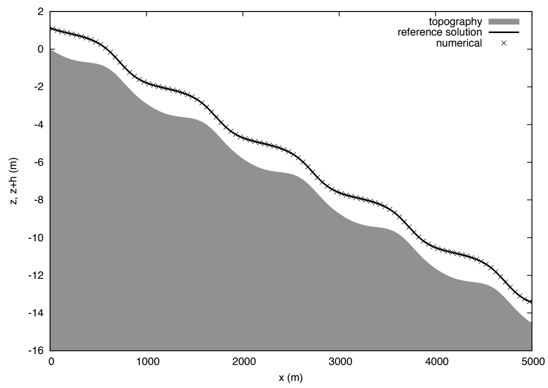

Figure 9: Test 4 - Periodic subcritical flow: water free surface at steady state. Manning-Chezy friction term is considered, with $n = 0.03$.

5.5. Subcritical flow

This test is very similar to the previous one. We consider a subcritical flow with a Manning-Chezy friction term (36). The purpose of this test is to perform qualitative comparisons with numerical results shown in [8]. As in the previous test, a reference solution can be obtained for steady state flows over varying topographies [24]. Considering a $150\,m$ long computational domain, the steady state for the free surface considered here is given by:

$$h_{ref}(x) = 0.8 + \frac{1}{4}\exp\left[-\frac{135}{4}\left(\frac{x-75}{150}\right)^2\right],$$

and we compute the corresponding topography as in §5.4. The steady discharge is constant on the whole domain and equal to $2\,m.s^{-1}$. Since the flow is subcritical both upstream and downstream, a discharge of $2\,m.s^{-1}$ is imposed at the left inlet boundary, while the water height is forced to $h_{ref}(150)$ at the right outlet boundary. The initial free surface is set to zero on the whole domain. The steady state configuration is shown on Figure 10. We show respectively on Figure 11 and 12 the comparison between numerical results and reference solutions for the steady state water height and discharge. In these computations, the CFL is set to 0.8, we use 50 points and the Manning friction coefficient is set to $n = 0.03$. We observe very close agreement between numerical results and the reference solution, with tiny oscillations around the steady state discharge. Let us remark that that the hydrostatic reconstruction used here is not explicitely designed to exactly preserve steady state with non-zero velocity. However, we obtained very satisfying results in the approximation of the steady discharge $hu = 2\,m.s^{-1}$.

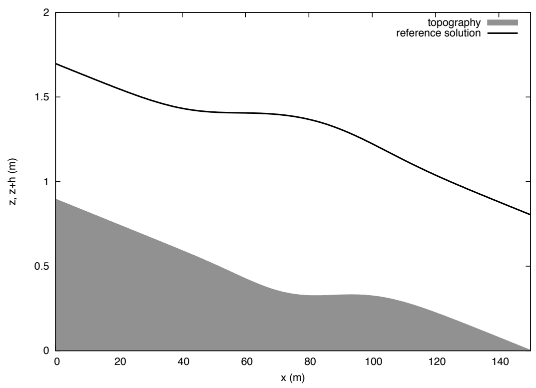

Figure 10: Test 5 - Subcritical flow: water free surface and topography at steady state with $n = 0.03$.

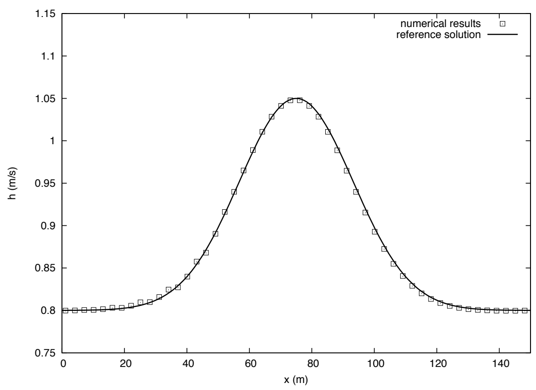

Figure 11: Test 5 - Subcritical flow: water height profile at steady state with $n = 0.03$.

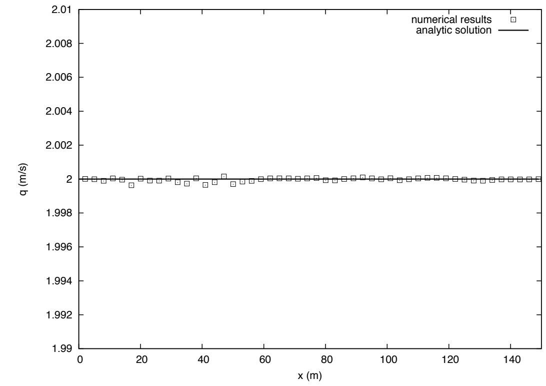

Figure 12: Test 5 - Subcritical flow: discharge profile at steady state with $n = 0.03$.

5.6. *Transcritical flow with shock*

In this last test, we consider a transcritical flow with a stationnary shock, for shallow water equations (36). Indeed, considering the steady state, the initial subcritical flow rapidly becomes super-critical, before coming back to a sub-critical evolution through a shock wave. We consider a $100\,m$ long computational domain and following [11], the steady free surface is defined by

$$h_{ref} = \begin{cases} \left(\frac{4}{g}\right)^{1/3}\left(\frac{4}{3} - \frac{x}{100}\right) - \frac{9x}{1000}\left(\frac{x}{100} - \frac{2}{3}\right), \text{ if } 0 \leq x \leq \frac{200}{3}\,m, \\ \left(\frac{4}{g}\right)^{1/3}\Big(\alpha_4\left(\frac{x}{100} - \frac{2}{3}\right)^4 + \alpha_3\left(\frac{x}{100} - \frac{2}{3}\right)^3 - \alpha_2\left(\frac{x}{100} - \frac{2}{3}\right)^2 \\ \qquad + \alpha_1\left(\frac{x}{100} - \frac{2}{3}\right) + \alpha_0\Big), \text{ if } \frac{200}{3} < x \leq 100\,m, \end{cases}$$

with $\alpha_0 = 1.4305$, $\alpha_1 = 14.492$, $\alpha_2 = 21.7112$ and $\alpha_4 = \alpha_3 = 0.674202$.
The corresponding topography is computed as in §5.4, and the steady discharge is $2\,m.s^{-1}$. Again, the initial free surface and discharge are set to zero on the whole domain, a discharge of $2\,m.s^{-1}$ is imposed at the left inlet boundary, while the water height is forced to $h_{ref}(100)$. The CFL is set to 0.8, we use 600 points ($dx = 0.166\,m$) and the Manning friction coefficient is set to $n = 0.0328$. Note that the number of cells is chosen to ensure an accurate computation of the shock location.
We can clearly see on Figure 13 that the flow accurately converges towards the steady state and that the shock location is accurately computed. The numerical results concerning the discharge are similar to those shown on Figure 12.

Acknowledgment

The authors wish to thank O. Delestre for his contribution.

References

[1] E. Audusse, F. Bouchut, M.O. Bristeau, R. Klein, and B. Perthame. A fast and stable well-balanced scheme with hydrostatic reconstruction for shallow water flows. *SIAM J. Sci. Comput.*, 25(6):2050–2065, 2004.

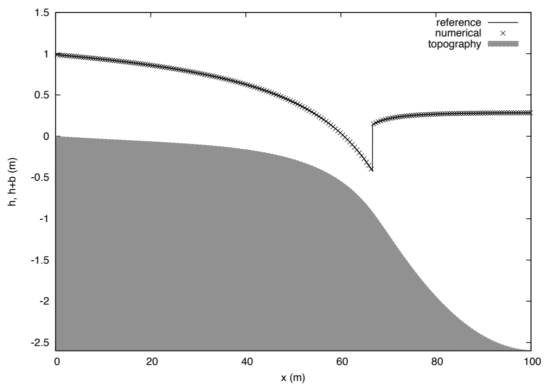

Figure 13: Test 6 - Subcritical flow over a bump: water free surface at steady state, with $n = 0.0328$.

[2] P. Batten, N. Clarke, C. Lambert, and D.M. Causon. On the choice of wavespeeds for the HLLC Riemann solver. *SIAM J. Sci. Comput.*, 18(6):1553–1570, 1997.

[3] C. Berthon, J. Dubois, B. Dubroca, T.-H. Nguyen-Bui, and R. Turpault. A free streaming contact preserving scheme for the M_1 model. *Adv. Appl. Math. Mech.*, 2(3):259–285, 2010.

[4] C. Berthon and F. Marche. A positive preserving high order VFRoe scheme for shallow water equations: a class of relaxation schemes. *SIAM J. Sci. Comput.*, 30(5):2587–2612, 2008.

[5] C. Berthon and R. Turpault. Asymptotic preserving hll schemes. *Numerical Methods for Partial Differential Equations,*.

[6] F. Bouchut. *Nonlinear stability of finite volume methods for hyperbolic conservation laws and well-balanced schemes for sources*. Frontiers in Mathematics. Birkhäuser Verlag, Basel, 2004.

[7] M.O. Bristeau and B. Perthame. Kinetic schemes for solving Saint-Venant equations on unstructured grids. In *Innovative methods for numerical solutions of partial differential equations (Arcachon, 1998)*, pages 267–277. World Sci. Publ., River Edge, NJ, 2002.

[8] J. Burguete, P. Garcia-Navarro, and J.Murillo. Friction term discretization and limitation to preserve stability and conservation in the 1d shallow-water model: application to unsteady irrigation and river flow. *Int. J. Numer. Meth. Fluids*, 58:403–425, 2008.

[9] M.J. Castro, A. Pardo, C. Parés, and E.F. Toro. On some fast well-balanced first order solvers for nonconservative systems. *Math. Comp.*, 79(271):1427–1472, 2010.

[10] C. Chalons, F. Coquel, E. Godlewski, P.A. Raviart, and N. Seguin. Godunov-type schemes for hyperbolic systems with parameter dependent source. the case of euler system with friction. *submitted*, 2010.

[11] O. Delestre. Simulation du ruisselement d'eau de pluie sur des surfaces agricoles. *P.h.D Thesis*, 2010.

[12] O. Delestre and F. Marche. A numerical scheme for a viscous shallow water model with friction. *Journal of Scientific Computing*, DOI: 10.1007/s10915-010-9393-y, 2010.

[13] A.-A. Flamant. *Mecanique Appliques - Hydraulique*. Baudry et Cie, 1891.

[14] T. Gallouët, J.M. Hérard, and N. Seguin. Some approximate Godunov schemes to compute shallow-water equations with topography. *Comput. & Fluids*, 32(4):479–513, 2003.

[15] E. Godlewski and P.A. Raviart. *Numerical approximation of hyperbolic systems of conservation laws*, volume 118 of *Applied Mathematical Sciences*. Springer-Verlag, New York, 1996.

[16] J.M. Greenberg and A.Y. LeRoux. A well-balanced scheme for the numerical processing of source terms in hyperbolic equations. *SIAM Journal on Numerical Analysis*, (1):1–16.

[17] A. Harten, P.D. Lax, and B. Van Leer. On upstream differencing and Godunov-type schemes for hyperbolic conservation laws. *SIAM Rev.*, 25(1):35–61, 1983.

[18] S. Jin. A steady-state capturing method for hyperbolic systems with geometrical source terms. *M2AN Math. Model. Numer. Anal.*, 35(4):631–645, 2001.

[19] C.Y. Kuo, Y.C. Tai, F. Bouchut, A. Mangeney, M. Pelanti, R.F. Chen, and K.J. Chang. Simulation of tsaoling landslide, taiwan, based on saint venant equations over general topography. *Engineering Geology*, 104(3-4):181 – 189, 2009.

[20] B. Van Leer. Towards the ultimate conservative difference scheme v. a second order sequel to godunov's method. *J. Comput. Phys.*, 32:101–136, 1979.

[21] Randall J. LeVeque. *Finite volume methods for hyperbolic problems*. Cambridge Texts in Applied Mathematics. Cambridge University Press, Cambridge, 2002.

[22] R.J. LeVeque and M. Pelanti. A class of approximate Riemann solvers and their relation to relaxation schemes. *J. Comput. Phys.*, 172(2):572–591, 2001.

[23] Q. Liang and F. Marche. Numerical resolution of well-balanced shallow water equations with complex source terms. *Advances in Water Resources*, 32(6):873–884, 2009.

[24] I. MacDonald, M.J. Baines, and N.K. Nichols ans P.G. Samuels. Analytic benchmark solutions for open channel flows. *ASCE Journal of Hydraulic Engineering*, 123:1041–1045, 1997.

[25] S. Noelle, N. Pankratz, G. Puppo, and J.R. Natvig. Well-balanced finite volume schemes of arbitrary order of accuracy for shallow water flows. *J. Comput. Phys.*, 213(2):474–499, 2006.

[26] J. Sampson, A. Easton, and M. Singh. Moving boundary shallow water flow above parabolic bottom topography. *ANZIAM J. (EMAC 2005)*, 47:373–387, 2006.

[27] J. Sampson, A. Esaton, and M. Singh. Moving boundary shallow water flow in a region with quadratic bathymetry. *ANZIAM J.*, 49:666–680, 2008.

[28] E. F. Toro, M. Spruce, and W. Speare. Restoration of the contact surface in the hll riemann solver. *Shock waves*, 4:25–34, 1994.

[29] E.F. Toro. *Riemann solvers and numerical methods for fluid dynamics*. Springer-Verlag, Berlin, second edition, 1999. A practical introduction.

[30] Y. Xing and C.W. Shu. High-order well-balanced finite difference weno schemes for a class of hyperbolic systems with source terms. *Journal of Scientific Computing*, 27(1-3):477–494, 2006.